JETIR.ORG ISSN: 2349-5162 | ESTD Year : 2014 | Monthly Issue
JOURNAL OF EMERGING TECHNOLOGIES AND INNOVATIVE RESEARCH (JETIR)
An International Scholarly Open Access, Peer-reviewed, Refereed Journal

Effect Of Additive Friction Stir Processing and Post Process Aging Treatment on Microstructure, Mechanical Properties and Electrical Conductivity of AA7075.

Kedar Joshi, Pranav Jadhav, Rohit Raut, Mayur Rawal, Hemant Deore
Department of Mechanical Engg. SKNCOE, SPPU PUNE.

Abstract - The aim of this paper is to study the effect of Additive friction stir processing (AFSP) on AA7075 to characterized the parameters like microstructure mechanical properties and electrical conductivity for applications in defence, aerospace, aircraft and many other industries due to its specific properties including a high strength- to-weight ratio and comparatively good mechanical properties in comparison to the other metals and alloys. In this research work the conductivity is measured using the van der pauw (VDP) method to find out the electrical conductivity. The Variations in Mechanical and Electrical properties is in the trend of the material added by AFSP. The enhancement in the mechanical and electrical properties was primarily ascribed to grain refinement, Zener pinning effect (attributable to incorporation of filler material) and precipitate evolution during subsequent age hardening.

Keywords – Additive Friction stir processing, Electrical Conductivity, Van dar pauw, Vickers Hardness.

Introduction

Several industries such as defence, aerospace, automobile and marine are on the lookout for novel means to minimize their costs, decrease the weight of their goods and increase their overall energy efficiency. Hence, light metal alloys of aluminium (Al) are taken into consideration as promising replacements for steels and other high density structural materials. Innovations in the field of alloy design and surface technologies has opened new dimensions for product designers and engineers to utilize light metal alloys in manners that would formerly have been deemed unsuitable.

The important characteristic of these techniques is external dimensions of the work- piece do not change during and after the processing. HPT- high pressure torsion [1], TE
–twist extrusion [2], ECAP – equal channel angular extrusion/pressing [4], FSP – friction stir processing, MDF – multi directional forging [5], RCS – repeated corrugation and straightening [6] and ARB –accumulative roll bonding [7] are some of the examples SPD techniques. Less heat generation, mechanical mixing, extensive material flow, large forging pressure, ultrafine grain structure and random misorientation of grain boundaries are the unique features of FSW, utilized by Mishra et al. Rotational (rpm) and traverse (mm/min) speed of tool tilt angle (°), plunge depth (mm) and tool geometry are the key process parameters of the FSP technique.

Poor surface attributes such as hardness, wear and abrasion resistance of these alloys is major concern, which limits their applicability in few areas like armour plates, bio-implants, shape memory alloys requiring high surface performance [8]. The surface quality level of Al based alloys can be improved by incorporation (reinforcement) of second phase particles to form surface composites. Various techniques like laser melt induction (LMI), vacuum arc melting (VAM), high-energy electron beam melting (EBM) [9] and few other has been used to produce surface composites on Al alloy substrates, however, problems associated with re-solidification of molten metal viz. dissolution of reinforcement, compositional segregation, grain coarsening,

cracking and porosity deteriorate properties of surface layer [10]. These problems can be unravelled by using friction stir processing (FSP), a solid-state metal processing technique, to fabricate surface composites [11]. Additive friction stir processing (AFSP) is state of the art surface modification method for fabrication of surface composite, which integrates reinforcement addition with FSP to indigenously alter chemical composition together with microstructure, with the intension of improving surface properties while keeping the bulk unimpaired.

Table 1.1 shows the Chemical Composition of AA7075 utilized for this research work.

Table 1

Chemical composition of as received AA7075-T6.

Material	%Mg	%Mn	%Zn	%Fe	%Cu	%Si	%Cr	%Al
AA7075-T651	2.1	0.12	5.1	0.32	1.2	0.58	0.078	Balance

Experimental Work

3.1 Additive Friction Stir Processing

The process starts with the sample preparation for the Additive Friction Stir Processing of AA7075 in T6 condition. The 180*120 mm and thickness of 6mm sample was cut for the further process. The array of 320 cylindrical holes of 2mm diameter and 3mm of depth were drilled on the surface area of specimen shown in Fig.3.1 The Additive Material of three different types was filled in that holes drilled having the avg length and diameter of MWCNT 15–20 nm and 5 μm respectively, the CU and sic Particles of average diameter of 25 μm and 10–20 μm respectively.

Fig.3.1 Arrangement and Drilling of hole for incorporating the additive materials.

The CNC FSW machine shown in Fig.3.2 was utilized to perform this process having capacity to produce the downward force of 10KN and speed up to 3000 rpm. The Tool Made of W-1% La2O (Tungsten-Lanthanum Oxide) alloy which is durable, rotating and having conical probe with 3mm pin length and 20mm shoulder diameter was selected for the further processing. The tool geometry is shown in Fig.3.3.

To Achieve the zero-defect processing the tool was plunged into the surface of the specimen up to 0.3 mm at higher rpm (1200 rpm) and 15 sec kept in that position for achieving required preheating. The processing was done on 800 rpm and the transverse speed of 60mm/min with tool tilt of 3 deg.

The Volume fraction of reinforcement was 5% with respect to the base metal. The filler particles were filled into the cavities by manually with the help of flat heat punch of 1.5mm. The AFSP was performed with the overlapping of 60% between the two successive passes to achieve the Equal Distribution shown in Fig.3.4. After the final

solution treatment (AFSP), artificial age hardening was carried out at 120 °C for 24 hours, followed by air cooling to room temperature. The artificial aging was utilized in the Electric Furnace shown in Fig3.5.

Fig.3.4 AFSPed Specimen with 60% overlap

3.2 Sample Preparation for Microstructure and Hardness Test

Samples were extracted from the region that underwent the Final Solution Treatment (AFSP) using an abrasive cut-off machine for the Metallography Examination Fig3.4. a and 3.4.b. After cutting the samples on abrasive cut-off machine samples of same dimensions were cut using Diamond Cutter as shown in Fig.3.5 the cutting speed was 80 to 120 rpm.

Fig.3.4. (a) Abrasive Cutt-Off Machine

Fig.3.4. b. Abrasive Cutt-Off Machine

Fig.3.5. Diamond Wheel Cutt-Off Machine

To observe the microstructure the specimens were polished on Polishing Machine as shown in Fig.3.6. The papers used for polishing were 2000,1500,1000,500 and 400.

Fig.3.6. Polishing Machine

For Etching and inspecting the microstructure of the specimens the samples were polished till the mirror finish and etched with the Keller reagent which contains (2 ml HF + 3mlHCl + 5 ml HNO3 + 190 ml H2O) [11]. The OM and SEM was performed to characterise the microstructural modifications like evenly mixing of reinforcement particles, changes in the grains structure and observing the grain morphology.

3.3 Microstructure and Hardness Test

Leica DMC 4500 was employed for optical microscopy, while Carl ZEISS FESEM with backscattered imaging mode was utilized for electron microscopy. Microhardness readings (a minimum of eight readings per specimen) were obtained to assess the degree of hardening by applying a load of 100 grams for 10 seconds (Fig.3.7).

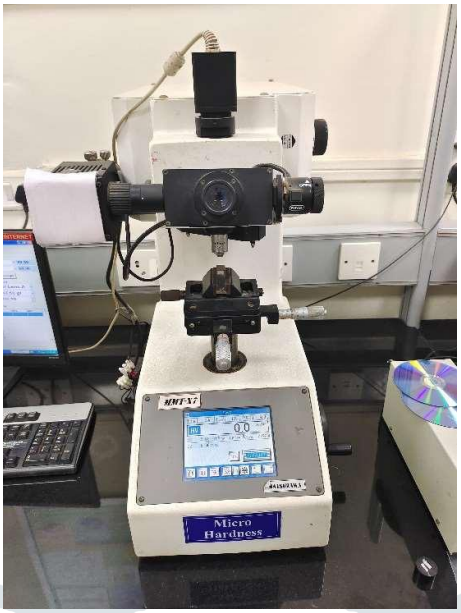

Fig.3.7. Micro-Hardness Test Setup

3.4 Wear Test

The ASTM G99-05 standard was followed for pin-on-disc wear tests using the DUCOM TR-20LE rotary tribometer. Prismatic specimen pins, sized 5 × 5 mm², were segmented from the FSPed area and tested against a hardened steel disk (60 HRC). Prior to testing, the wear test specimens were prepared by polishing with 1200-grit sandpaper, followed by polishing using 3 µm diamond paste. The wear test was conducted with a nominal load of 30 N, a sliding speed of 1 m/s, and a sliding distance of 600 m [12]. Mass differences, measured with an accuracy of 0.1 mg, were used to calculate wear loss before and after each test. The rate of wear was measured using the weight reduction by the following equation,

$$Wa = \frac{\Delta m}{M \times s \times \rho}$$

where, Wa corresponds to wear rate, Δm corresponds to weight loss (g), M corresponds to applied load (N), and ρ corresponds to density (g/ cm3).

3.5 XRD Measurements

Friction stir processed surface, were used for XRD measurements. Calculation of lattice strains was done from the slopes of sinθ vs Bcosθ using WeH (Williamson-hall) plots, where B2 = Br 2 – Ba 2 . Br and Ba are full width half maxima (FWHM) for measured and standard samples respectively and θ is the Bragg angle [13,14].

3.6 Electrical Conductivity

The Vander Pauw Method was employed to characterize the electrical conductivity of both the base metal and the Fsped alloy, incorporating various reinforcements. This characterization technique, known as the Hall Effect Measurement System, was utilized for the assessment [15].

The Ecopia HMS-3000 (Fig.3.7) apparatus facilitated the execution of this process, boasting accuracy up to Mega readings. Samples, crafted to dimensions of 10mm x

10mm and a thickness of 1mm, underwent preparation via the Double Disk Polishing

Machine to achieve a mirror-like finish and a precisely flat surface.

Fig.3.8. The Ecopia HMS-3000

Upon placement onto a flat plate, the samples were connected at their four corners with the four wires of the setup, as depicted in the figure. A current was passed through one side of the samples while voltage measurements were taken across the opposite side, as illustrated in the figure.

Current was varied in increments from 1mA to 12mA, with alternating sides of the sample. Resistance for each current pass was determined using Ohm's law equation V=IR. The calculation of resistivity was performed utilizing the formula:

$\rho = (\pi/\ln 2)\ (V/I) \times d$

Resistivity was also computed by multiplying the sheet resistance by the sample thickness. Conductivity was then derived using the relation in Siemens per cm:

$\sigma = 1/\rho$

Results and Discussion

4.1 Optical & SEM Microstructure

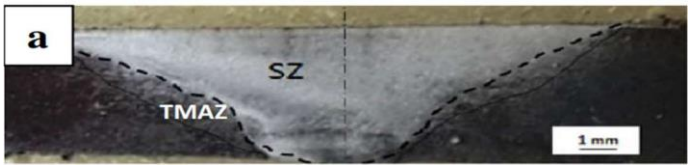

Fig. 4.1 (a) Macrostructure after AFSP, Optical Microstructures showing (b) Base Metal AA7075 T6, (c) Stir Zone of AFSPed AA7075 without filler, (d) Stir Zone of AFSPed AA7075 with MWCNT filler (e) Stir Zone of AFSPed AA7075 with Cu filler, (f) Stir Zone of AFSPed AA7075 with Sic filler

Essentially, the microstructure of Friction Stir Processing (FSP) exhibits three clear regions: the stir zone (SZ), the thermo-mechanically affected zone (TMAZ), and the heat affected zone (HAZ).

Figure 4.1 (a) illustrates the macrostructure of the FSPed specimen, displaying the sizes of the SZ (Stir Zone) and TMAZ (Thermo-Mechanically Affected Zone). In this current

study, particular emphasis was placed on the microstructural analysis of the stir zone

(SZ).
Figure 4.1 (b) illustrates the optical microstructures of the base material (AA7075), characterized by elongated grains with a mean diameter ranging from 50 to 80 µm. Additionally, a scattering of large irregular-shaped particles, measuring 5–10 µm in size, is evident. These particles predominantly comprise Al-Cu compounds, along with other alloying elements. These particles are often called "constituent" particles and exhibit high resistance to dissolution. [16].

In comparison, the microstructure of the FSPed stir zone, without the addition of any filler material (as shown in Fig. 4.1(c)), exhibits dynamically recrystallized fine, equiaxed grains. This phenomenon is attributed to the collective effects of frictional heating and intense plastic deformation. Considering to several researchers, a variety of restoration mechanisms such as dynamic recovery (DRV), discontinuous dynamic recrystallization (DDRX), continuous dynamic recrystallization (CDRX), [17] and geometric dynamic recrystallization (GDRX) [18] are responsible for the development of a fine-grained microstructure in aluminium alloys during FSP.

During friction stir processing (FSP), the rotating and traversing motion of the tool combines and blends both the base material and filler particles together. As the overlap ratio and number of passes increase, filler particles disperse more evenly [19].

In the Fsped sample of MWCNT (depicted in Fig. 4.1(d)), we observed a uniform distribution and coalescing deposition. However, in the surface composite of Cu and Sic additives, an incomplete or partial pattern of coalescing deposition was evident ashown in fig.4.1 (e)&(f). The variance in this pattern could be attributed to variations in the size and individual adaptability of the filler materials.

The microstructural characteristics of the AFSPed stir zone were examined under SEM at two different magnifications, as shown in Fig. 4.2 The three surface composites exhibit a well-dispersed arrangement of filler particles. In Figure 4.2 (a), an enlarged SEM depiction of an Al-MWCNT composite sample displays fragmented and clustered MWCNT aggregates, verified by energy-dispersive X-ray spectroscopy (EDS). This observation implies that the MWCNTs have fractured as a result of the stirring and mixing actions during Friction Stir Processing (FSP), corroborating findings from prior research on FSP employing CNT additives [20]. Intermetallic formations of Al-Cu are evident in certain regions, alongside fragmented particles visible in the SEM image of the Cu filler, as depicted in Figure 4.2 (b). The scanning electron microscope (SEM) micrograph of the Friction Stir

Processed (FSPed) sample, shown in Figure 4(c), vividly illustrates the fragmentation and uniform dispersion of silicon carbide (Sic) reinforcement particles. These particles exhibit strong interfacial bonding with the aluminium (Al) matrix. The observation confirms that the significant plastic strain induced during FSP leads to the fragmentation of Sic particles into multiple smaller fragments. Additionally, due to the material flow characteristics of FSP, these particles are evenly distributed throughout the Al matrix. The Fig 4.2 (d) shows the precipitation formation of MgZn2 and Al2Cu due to the aging at 120 C which significantly improves the hardness and wear resistance.

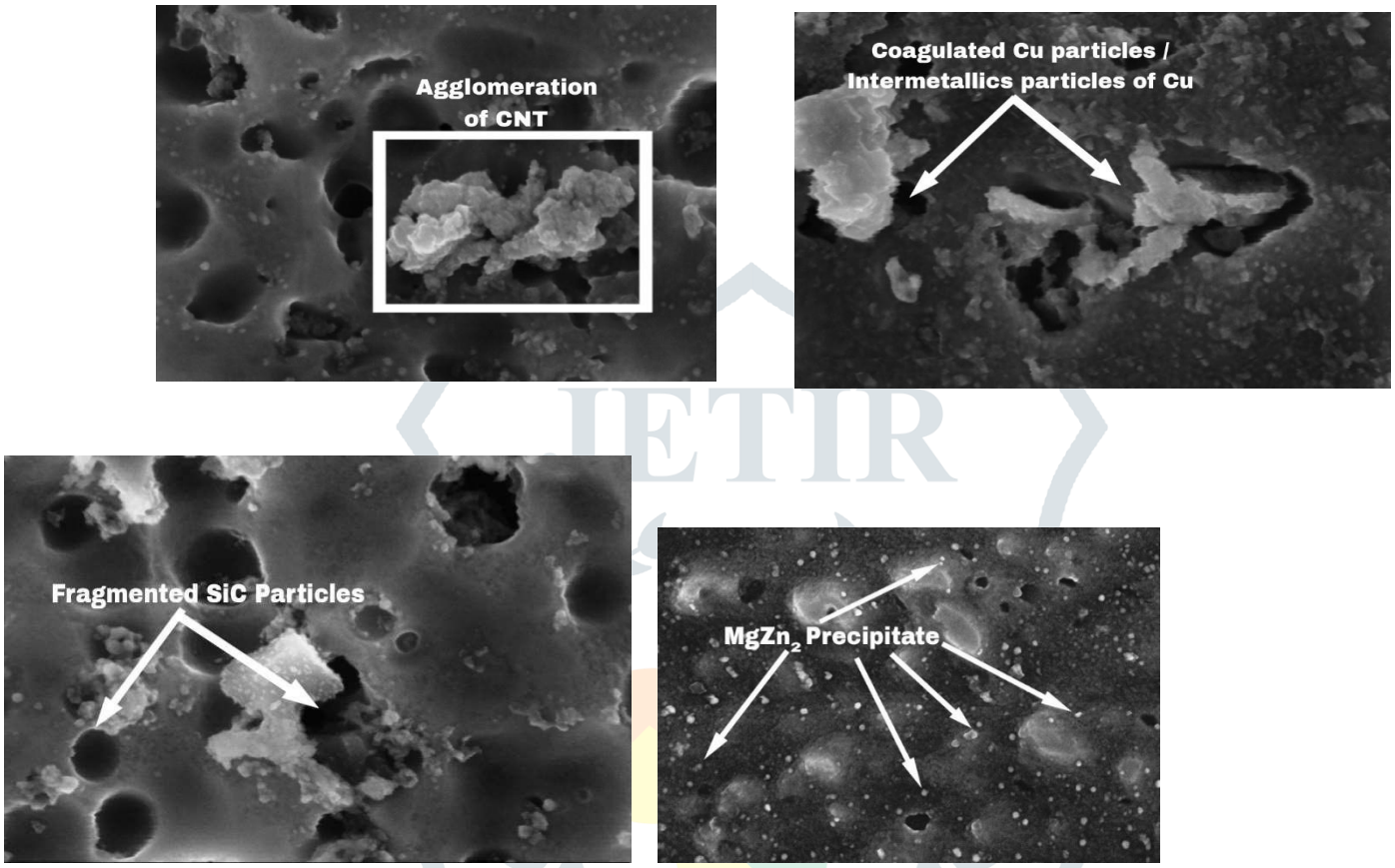

Fig. 4.2 SEM of (a) Agglomeration of MWCNT in Al Matrix (b) Coagulated and intermetallic of Cu filler (c) Fragmentation of Sic Filler particles (d) Precipites of MgZn2 formed during aging confirmed by XRD.

4.2 X-ray diffraction

The XRD pattern of the base, FSPed with MWCNT, SiC and Cu fillers and post process age hardened at 120 °C are shown in Fig. 4.3 (a). The presence of Sic (JCPDS 49–1623) and Cu (JCPDS 04–0836) phases are clearly revealed in XRD results. However, absence of Al4C3 phase peak indicates no reaction of CNT with Al Matrix. According to the literature referenced in this study, the XRD patterns of the post-process age- hardened samples exhibit peaks corresponding to MgZn2. Significant variations in peak widths and positions were observed among samples processed under different conditions.

Fig 4.3(a) XRD scans depicting intensity versus 2θ for various processing conditions are presented. The positions of key peaks such as primary Al, MgZn2 precipitate, Sic, and Cu are highlighted for reference.

4.3 Mechanical Properties

4.3.1 Hardness

Figure 4.4 (a) depicts the average hardness of the base metal in the T6 condition, as well as the hardness variations following the AFSP and post-FSP aging treatments. The base metal exhibited a hardness of 138. Notably, after friction stir processing (FSP) without any reinforcement, the hardness increased to 145. This enhancement can be attributed to ultrafine grain refinement and an increase in dislocation density. Duringmthe FSP, intense heat generation leads to the mechanical rupture of inherent grain boundaries, followed by dynamic recrystallization, resulting in the formation of ultrafine grains.

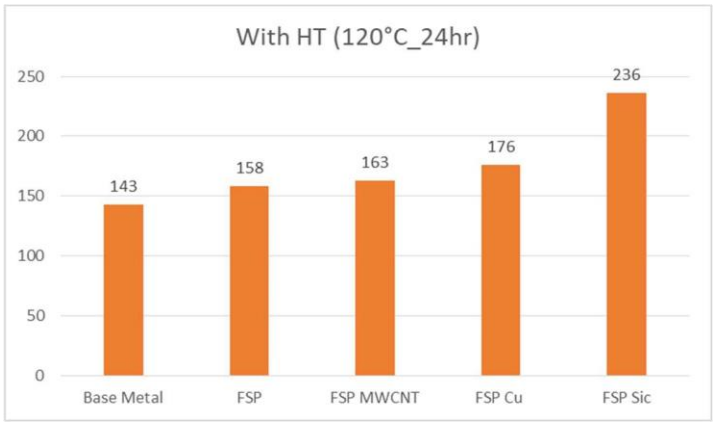

Fig 4.4 (a) average hardness comparison of BM AA7075T6, plain FSP and Different fillers without aging (b) average hardness comparison of BM AA7075T6, plain FSP and Different fillers with aging.

The significant enhancement in the hardness of the Sic specimen is primarily a result of the increased grain boundary area, leading to heightened hardness. This improvement stems from two main factors: dispersion strengthening induced by Sic particles and grain refinement occurring during friction stir processing (FSP) in the alloy filled with Sic filler. The inclusion of Sic particles leads to more pronounced localized deformation and grain fragmentation than what is observed with MWCNT and Cu particles. This is because the hardness value decreases in the order of Sic, followed by MWCNT, and then Cu.

Figure 4.4 (b) displays the influence of age hardening on the average hardness of surface composites processed through Friction Stir Processing (FSP) using various fillers. Among them, the surface composite with Sic filler showcased the highest average hardness, followed by the composite with Cu filler showing intermediate hardness, and the one with MWCNT filler displaying the least hardness. Notably, significant hardness enhancement was evident across all three surface composites incorporating different fillers (Sic, MWCNT, and Cu) due to the formation of precipitates (MgZn2) during the aging treatment. This increase is attributed to low- temperature aging and extended holding times, which activate homogeneous nucleation sites, facilitating the formation of uniformly distributed spherical precipitates within the matrix.

4.3.2 Wear Behaviour

The **wear resistance**, as measured by **wear loss**, of both the base metal and surface composites fabricated using different fillers through Friction Stir Processing (FSP) is depicted in **Figure 4.4 (c)** Incorporating filler particles improves wear resistance. Among the fillers, Sic and MWCNT have the strongest and weakest influence on enhancing wear resistance, respectively, while Cu filler falls in between. Figure 11(a) illustrates the impact of post-FSP (Friction Stir Processing) age hardening on the wear resistance of surface composites prepared by FSP. After age hardening, the wear resistance of surface composites further increases due to the formation of hard and wear-resistant intermetallic compounds (precipitates) uniformly distributed in the matrix. Interestingly, the base metal (AA7075 T6) experiences higher wear loss, whereas the FSPed and subsequently age-hardened surface composites exhibit lower wear loss. The highest wear resistance is observed in the age-hardened Sic surface composite. As discussed in the microstructure section, the age-hardened Sic surface composite features fragmented hard Sic particles and tiny MgZn2 precipitates evenly dispersed in the Al matrix, resulting in excellent interfacial bonding and enhanced wear resistance

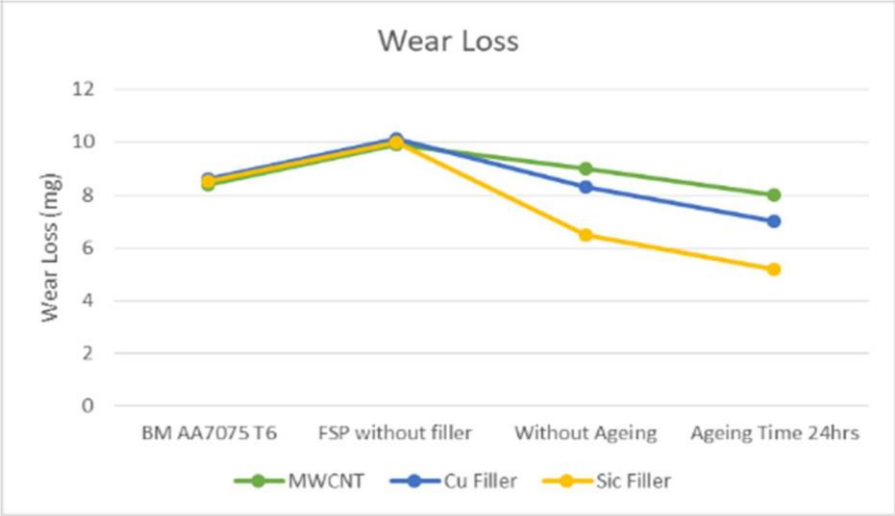

Fig 4.4(c) Wear Loss during pin on disc wear test carried out with Load 30 N, Sliding Distance 600 m, Sliding speed 1 m/s.

4.3 Electrical Conductivity

The electrical properties, such as sheet resistance, resistivity, and electrical conductivity, were determined using the Vander Pauw method, as illustrated in Figure
4.5. Following aging, the Multi-Walled Carbon Nanotubes (MWCNT) exhibited the highest electrical conductivity at 2.19 × 10^7 S/m, attributed to carbon's excellent conductivity. This outcome suggests significant coalescing deposition of MWCNT. Moreover, the formation of precipitates in the Fsped specimen of MWCNT during aging treatment was minimal, correlating with its lowest hardness value compared to Sic and Cu. Conversely, MWCNT without aging demonstrated a gradual decrease in conductivity due to the clustering and agglomeration of filler particles on the surface composite.

The conductivity of the base metal is measured at 1.68 × 10^7 S/m, which falls below that of MWCNT but surpasses all Fsped specimens of Sic and Cu, both with and without aging. Interestingly, the inclusion of Cu filler results in decreased conductivity compared to the base metal, as well as the Fsped alloy of MWCNT filler, despite copper's reputation as an excellent conductor of electrical current. This phenomenon is attributed to the formation of intermetallic of Al-Cu during the FSP process and subsequent aging, leading to the formation of precipitates that lower the electrical conductivity while enhancing hardness relative to the base metal and MWCNT filler.

The electrical conductivity of the aged friction stir processed (FSP) copper filler specimen is measured at 1.49 × 10^7 (S/m), while the non-aged counterpart exhibits a value of 1.45 × 10^7 (S/m), indicating comparable levels. However, the incorporation of ultrafine grain refinement during FSP, coupled with an increased dislocation density, leads to reduced conductivity in both aged (1.16 × 10^7 S/m) and non-aged (9.45 × 10^6 S/m) FSP specimens.

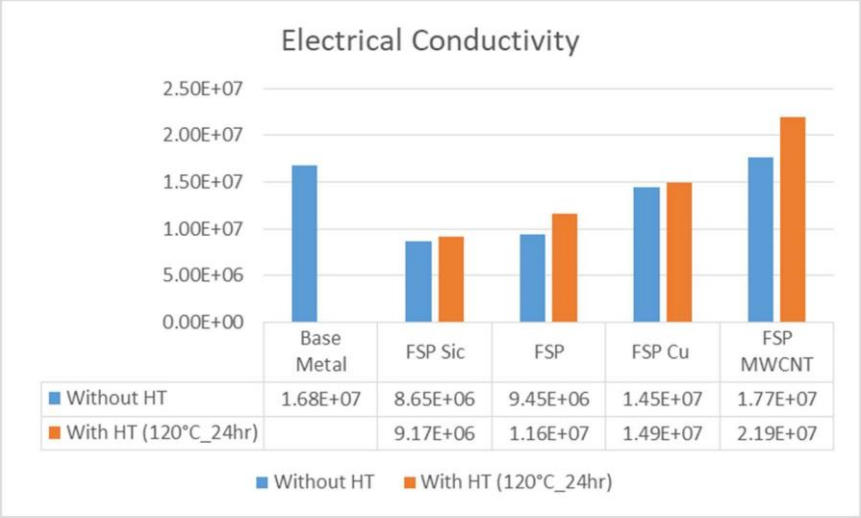

Fig 4.5 Electrical Conductivity trend comparison between with and without heat treatment of BMAA7075, FSP without filler and incorporating different fillers via FSP

The decline in conductivity observed in the Fsped alloy without aging stems from grain refinement and alterations in grain boundary conditions. Conversely, the notable increase in grain size and coarsening contributes to a modest enhancement in conductivity for the heat-treated Fsped specimen without any filler compared to the non-aged Fsped alloy.

Adding Sic filler results in the least conductivity compared to all specimens, regardless of heat treatment. This is because silicon isn't a proficient conductor of electricity.

Additionally, the dispersion strengthening from Sic particles and the grain refinement from Fsp contribute to this effect.

The heightened hardness reflects the decreased conductivity of the Fsped Sic specimen, both with and without aging, measured at 9.17E+06 and 8.65E+06 respectively. This is attributed to precipitate formation during heat treatment and heightened resistance to dislocation within the material.

Conclusion

Surface composites based on AA 7075, strengthened with MWCNT, Cu, and SiC fillers, have been effectively produced using FSP. The comparative impact of various filler materials and subsequent age hardening on the microstructural modification, mechanical property variation, and wear behaviour of aluminium matrix surface composites fabricated via FSP were identified and summarized below.

1. Significant grain refinement was observed in surface composites processed via FSP
2. Post-process age hardening led to the formation of MgZn2 precipitates in all three surface composites manufactured via FSP, which included MWCNT, Cu, and Sic fillers.
3. The addition of filler materials notably enhanced the microhardness and wear resistance. These properties were further augmented through post-process age hardening.
4. Among the three fillers investigated under the set FSP and age hardening parameters, sic filler emerged as the most effective. Age-hardened Sic filler surface composites exhibited nearly a twofold increase in microhardness, impact toughness, and wear resistance.
5. The obtained results for the electrical conductivity of the base metal, plain FSP, and FSP incorporating filler materials do not align with the expected outcomes. Variations in values may be attributed to factors such as insufficient filler material incorporation, extensive plastic deformation, and the formation of precipitates during aging.

References

[1]. Yu. Ivanisenko, R. Kulagin, V. Fedorov, A. Mazilkin, T. Scherer, B. Baretzky, H. Hahn, High pressure torsion extrusion as a new severe plastic deformation process, Mater. Sci. Eng. A 664 (2016) 247–256.
[2].H. Zendehdel, A. Hassani, Influence of twist extrusion process on microstructure and mechanical properties of 6063 aluminium alloy, Mater. Des.
37 (2012) 13–18.

[3]. R.Z. Valiev, T.G. Langdon, Principles of equal-channel angular pressing as a processing tool for grain refinement, Prog. Mater. Sci. 51 (7) (2006) 881–981
[4]. M. Hong, D. Wu, R.S. Chen, X.H. Du, Ductility enhancement of EW75 alloy by multi-directional forging, J. Magnes. Alloys 2 (4) (2014) 317–324.
[5]. P.M. Bhovi, D.C. Patil, S.A. Kori, K. Venkateswarlu, Yi Huang, T.G. Langdon, A comparison of repetitive corrugation and straightening and high-pressure torsion using an Al-mg-Sc alloy, J. Mater. Res. Technol. 5 (4) (2016) 353–359.
[6]. M.R. Toroghinejad, F. Ashrafizadeh, R. Jamaati, On the use of accumulative roll bonding process to develop nanostructured aluminum alloy 5083, Mater. Sci. Eng. A 561 (2013) 145–151.
[7]. D.P. Edwards, I.G. Crouch, Light alloys, The Sci. of Armour Materials (2017)

117-166
[8]. Yuting Lv, Z. Ding, X. Sun, L. Li, G. Sha, R. Liu, L. Wang, International

Journal of Nanomedicine 13 (2018)

[9]. R.S. Mishra, Z.Y. Ma, Material Science and Engineering: R: Reports 50 (2005)

1-78.

[10]. H. S. Arora, H. Singh, B. K. Dhindaw, The International Journal of Advanced Manufacturing Technology 61 (2012) 1043-1055.[11]R.S. Mishra, Z.Y. Ma, Friction stir welding and processing, Mater. Sci. Eng. R 50(2005) 1–
78.

[11]. H.A. Deore, J. Mishra, A.G. Rao, H. Mehtani, V.D. Hiwarkar,

Effect of filler material and post process ageing treatment on microstructure, mechanical properties and wear behaviour of friction stir processed AA 7075 surface composites, Surface and Coatings Technology, Volume 374,2019,Pages
52-64,ISSN 0257-8972, https://doi.org/10.1016/j.surfcoat.2019.05.048.

[12]. H.A. Deore, A. Bhardwaj, A.G. Rao, J. Mishra, V.D. Hiwarkar, Consequence of reinforced Sic particles and post process artificial ageing on microstructure and mechanical properties of friction stir processed AA7075, Defence Technology, Volume 16, Issue 5,2020, Pages 1039-1050, ISSN 2214-
9147, https://doi.org/10.1016/j.dt.2019.12.001.

[13]. G.K. Williamson, W.H. Hall, X-ray line broadening from filed aluminium and wolfram, Acta Metall. 1 (1953) 22–31.

[14]. C. Suryanarayana, M. Grant Norton, X-Ray Diffraction - a Practical

Approach, Plenum, London, 1998.

[15]. ELECTRICALRESISTIVITYMEASUREMENTS: AREVIEW,YADUNATH SINGH (India) International Journal of Modern Physics: Conference Series 2013 22: 745-756
[16]. H.V. Atkinson, K. Burke, G. Vaneetveld, Recrystallization in the semi- solid state in 7075 aluminium alloy, Mater. Sci. Eng. A 490 (2008) 266–276.
[17]. T.R. McNelley, S. Swaminathan, J.Q. Su, Recrystallization mechanisms during friction stir welding/processing of aluminum alloys, Scr. Mater. 58 (5) (2008) 349–354.
[18]. J.Q. Su, T.W. Nelson, C.J. Sterling, Grain refinement of aluminum alloys by friction stir processing, Philos. Mag. 86 (1) (2006) 1–24.
[19]. R. Yang, Z. Zhang, Y. Zhao, G. Chen, Y. Guo, M. Liu, J. Zhang, Effect of multi-pass friction stir processing on microstructure and mechanical properties of Al3Ti/A356 composites, Mater. Charact. 106 (2015) 62–69.
[20]. Z. Du, M.J. Tan, J.F. Guo, J. Wei, Friction stir processing of Al–CNT

composites, J. Mater. Des. Appl. 230 (3) (2016) 825–833